This is the accepted manuscript made available via CHORUS. The article has been published as:

Dynamic mass generation on two-dimensional electronic hyperbolic lattices

Noble Gluscevich, Abhisek Samanta, Sourav Manna, and Bitan Roy

Phys. Rev. B **111**, L121108 — Published 20 March 2025

DOI: 10.1103/PhysRevB.111.L121108

Dynamic mass generation on two-dimensional electronic hyperbolic lattices

Noble Gluscevich,[1,*] Abhisek Samanta,[2,3,*] Sourav Manna,[4,5] and Bitan Roy[1,†]

[1] *Department of Physics, Lehigh University, Bethlehem, Pennsylvania, 18015, USA*
[2] *Department of Physics, The Ohio State University, Columbus, Ohio 43210, USA*
[3] *Department of Physics, Indian Institute of Technology Gandhinagar, Gujarat 382355, India*
[4] *Department of Condensed Matter Physics, Weizmann Institute of Science, Rehovot 7610001, Israel*
[5] *Raymond and Beverly Sackler School of Physics and Astronomy, Tel-Aviv University, Tel Aviv 6997801, Israel*

Free electrons hopping on hyperbolic lattices embedded on a negatively curved space can foster (a) Dirac liquids, (b) Fermi liquids, and (c) flat bands, respectively characterized by a vanishing, constant, and divergent density of states near the half-filling. From numerical self-consistent mean-field Hartree analyses, we show that nearest-neighbor Coulomb and on-site Hubbard repulsions respectively give rise to charge-density-wave and antiferromagnetic orders featuring staggered patterns of average electronic density and magnetization in all these systems, when the hyperbolic tessellation is accomplished by periodic arrangements of even p-gons. Both quantum orders dynamically open mass gaps near the charge neutrality point via spontaneous symmetry breaking. Only on hyperbolic Dirac materials these orderings take place via quantum phase transitions (QPTs) beyond critical interactions, which however decreases with increasing curvature, showcasing curvature induced weak coupling QPTs. We present scaling of these masses with the corresponding interaction strengths.

Introduction. From table salts to quantum materials, crystals are ubiquitous in nature. They feature discrete translational, rotational and reflection symmetries, manifesting periodic arrangements of regular polygons with p arms (p-gon). Yet another integer plays a pivotal role for the geometric classification of crystals, the number of nearest-neighbor (NN) sites q, connected to each vertex of a p-gon. On Euclidean plane, these symmetry constraints lead to $(p-2)(q-2)=4$, permitting triangular ($2p=q=6$), square ($p=q=4$), and honeycomb ($p=2q=6$) lattices. By contrast, hyperbolic tessellation on a negatively curved space, is accomplished when an inequality $(p-2)(q-2)>4$ is satisfied. Therefore, hyperbolic space accommodates infinitely many periodic lattices, characterized by Schläfli symbol (p,q) [1–15].

Naturally, hyperbolic quantum materials harbor a variety of electronic band structures [6–14]. They can be classified in terms of the density of states (DOS) near half-filling or zero-energy. A family of hyperbolic lattices (HLs) with even integer p, constituting bipartite lattices with the NN sites belonging to A and B sublattices [Figs. 1 and 2], fosters (a) Dirac liquids, (b) Fermi liquids, and (c) flat bands depending on p and q, captured from a free electron tight-binding model with only the NN hopping between sites from to A and B sublattices. Respectively, they feature vanishing, constant, and divergent DOS at zero energy [$\rho(0)$]. See Table I.

On such electronic HLs with open boundary condition (OBC), we numerically investigate the role of NN Coulomb (V) and on-site Hubbard (U) repulsions at half-filling within the mean-field or Hartree approximation. Respectively, they support staggered patterns of electronic density and spin, two quantum phases named charge-density-wave (CDW) and antiferromagnet (AFM). While infinitesimal V and U are sufficient to nucleate them on HLs hosting Fermi liquids and flat bands, due to the linearly vanishing DOS such orderings take place at finite interactions via quantum phase transitions (QPTs) in Dirac liquids. See Fig. 1 and Fig. 2. More intriguingly, as the curvature is strengthened in Dirac materials (realized for larger p), the critical couplings for these two ordering decrease monotonically, indicating curvature induced weak coupling QPTs. See Fig. 3.

p-gon	Dirac liquid	Fermi liquid	Flat band
$p/2=$ odd	$q=3$	$q=4,5$	$\times$
$p/2=$ even	$\times$	$q=3$	$q=4,5$

TABLE I. Classification of electronic bipartitie (even p) HLs in terms of the DOS at zero energy $\rho(0)$. Dirac liquid, Fermi liquid, and flat band are identified from vanishing, constant, and divergent $\rho(0)$, respectively.

Free fermions. A tight-binding model of free fermions, hopping only between the NN sites of HLs, is given by

$$H_0=-\sum_{\langle i,j\rangle}t_{ij}c_i^\dagger c_j, \tag{1}$$

where $c_i^\dagger$ (c_i) is the fermionic creation (annihilation) operator on the ith site and $\langle\cdots\rangle$ restricts the summation within the NN sites [16]. The spin independent NN hopping amplitude t_{ij} is assumed to be constant t, which we set to be unity. For simplicity, we suppress the fermionic spin index. Inclusion of spin only causes a mere doubling of H_0. The Hamiltonian operator ($\hat{h}_0$) associated to H_0 preserves (a) time-reversal symmetry ($\mathcal{T}$): $\mathcal{T}\hat{h}_0\mathcal{T}^{-1}=+\hat{h}_0$ with $\mathcal{T}^2=+1$, (b) anti-unitary particle-hole symmetry ($\mathcal{P}$): $\mathcal{P}\hat{h}_0\mathcal{P}^{-1}=-\hat{h}_0$ with $\mathcal{P}^2=+1$, and (c) unitary chiral or sublattice sym-

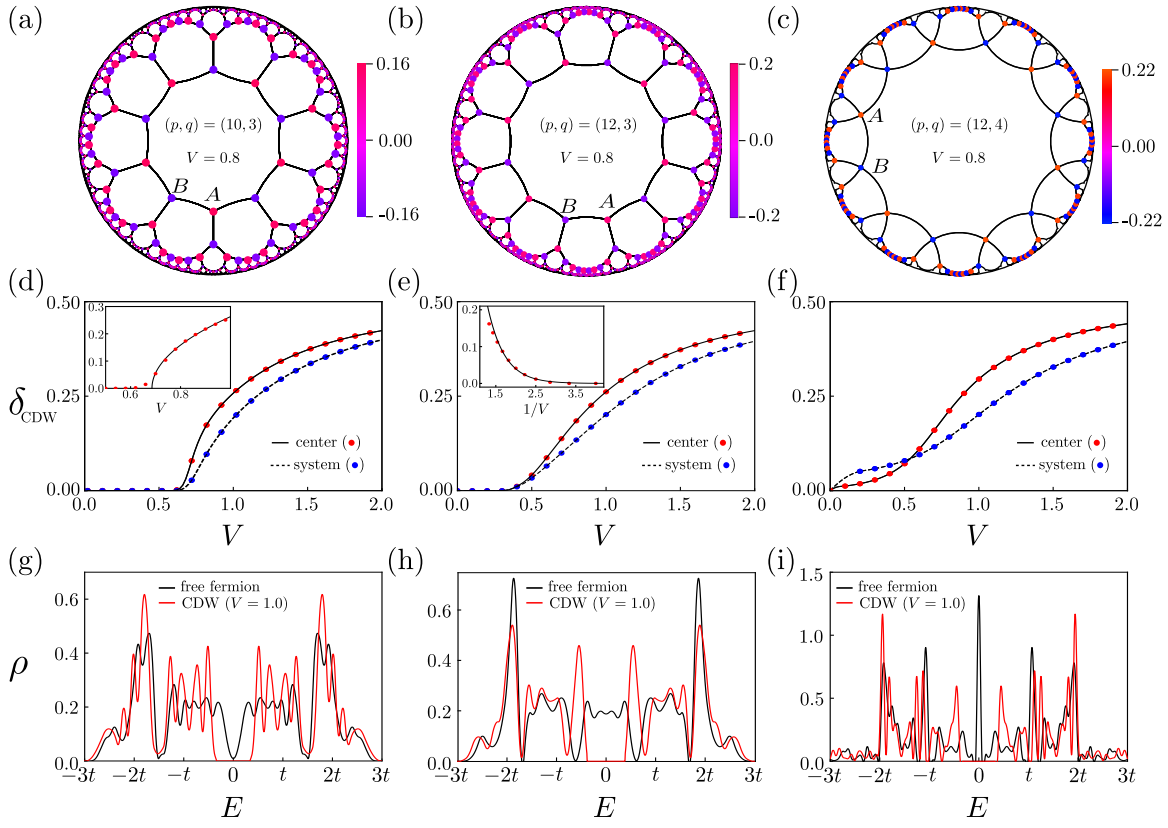


FIG. 1. CDW on HLs (shown on a Poincaré disk) resulting from the NN Coulomb repulsion (V). Spatial variation of the average electronic density measured from the half-filling on (a) $(10,3)$, (b) $(12,3)$, and (c) $(12,4)$ HLs for $V = 0.8$. Scaling of the CDW order parameter at the center, constituted by the sites belonging to the zeroth generation or center p-gon of the system [16] (red) and averaged over the entire system (blue) with V are shown in (d), (e), and (f), respectively. DOS for free fermions (black) and with the CDW order for $V = 1.0$ (red) are shown in (g), (h) and (i), respectively, displaying the formation of a mass gap. Here, the results are presented for third generation $(10,3)$, $(12,3)$, and $(12,4)$ HLs, respectively containing 2880, 7680, and 13080 sites [16]. Critical coupling for the CDW ordering in $(10,3)$ Dirac system is estimated to be $V_c \approx 0.69$ [inset of (d)], while in $(12,3)$ Fermi liquids it follows the BCS scaling [inset of (e)].

metry ($\mathcal{C}$): $\mathcal{C}\hat{h}_0\mathcal{C}^{-1} = -\hat{h}_0$ with $\mathcal{C}^2 = 1$. Hence, the system belongs to the class BDI [17, 18]. A half-filled system keeps all the negative (positive) energy states occupied (empty), and the average fermionic density at each site is 1/2, manifesting the sublattice exchange symmetry. Then $\rho(0)$ serves as a smoking gun probe to group quantum hyperbolic materials into three broad classes, characterized by vanishing (Dirac liquid), constant (Fermi liquid), and divergent (flat band) $\rho(0)$. See Table I. A slight deviation from a perfect $|E|$-linear DOS in hyperbolic Dirac materials very close to $E = 0$ results from finite size effects. DOS computed from hyperbolic band theory [8] shows a perfect $|E|$-linear behavior near $E = 0$ [18].

NN repulsion. We now investigate the role of electronic interactions in these three families of quantum fluids, first considering spinless fermions and NN Coulomb repulsion (V), captured by the Hamiltonian

$$H_V = H_0 + \frac{V}{2}\sum_{\langle i,j\rangle} n_i n_j - \mu N. \tag{2}$$

Here $n_i = c_i^\dagger c_i$ is the fermionic density on site i, N is the total number of spinless fermions in the half-filled system and μ is the chemical potential. Performing a Hartree decomposition of the quartic term, we arrive at the effective single-particle Hamiltonian [19–21]

$$H_V^{\rm Har} = H_0 + V\sum_{\langle i,j\rangle}\Big(\langle n_{B,i}\rangle n_{A,j} + \langle n_{A,i}\rangle n_{B,j}\Big) - \mu N. \tag{3}$$

Here $\langle n_A\rangle$ ($\langle n_B\rangle$) corresponds to the site dependent self-consistent average electronic density on the sublattice A (B). We measure them relative to the uniform density at half-filling: $\langle n_{A,i}\rangle = 1/2 + \delta_{A,i}$ and $\langle n_{B,i}\rangle = 1/2 - \delta_{B,i}$. Half-filling is maintained by choosing $\mu = V/2$ and ensuring that $\sum_i (\delta_{A,i} - \delta_{B,i}) = 0$. Positive definite quantities δ_A and δ_B yield the local CDW order parameter

$$\delta_{\rm CDW} = \frac{1}{2}(\delta_A + \delta_B), \tag{4}$$

where for a given A site, the B site is one of the two NN sites belonging to the same generation of the hyperbolic

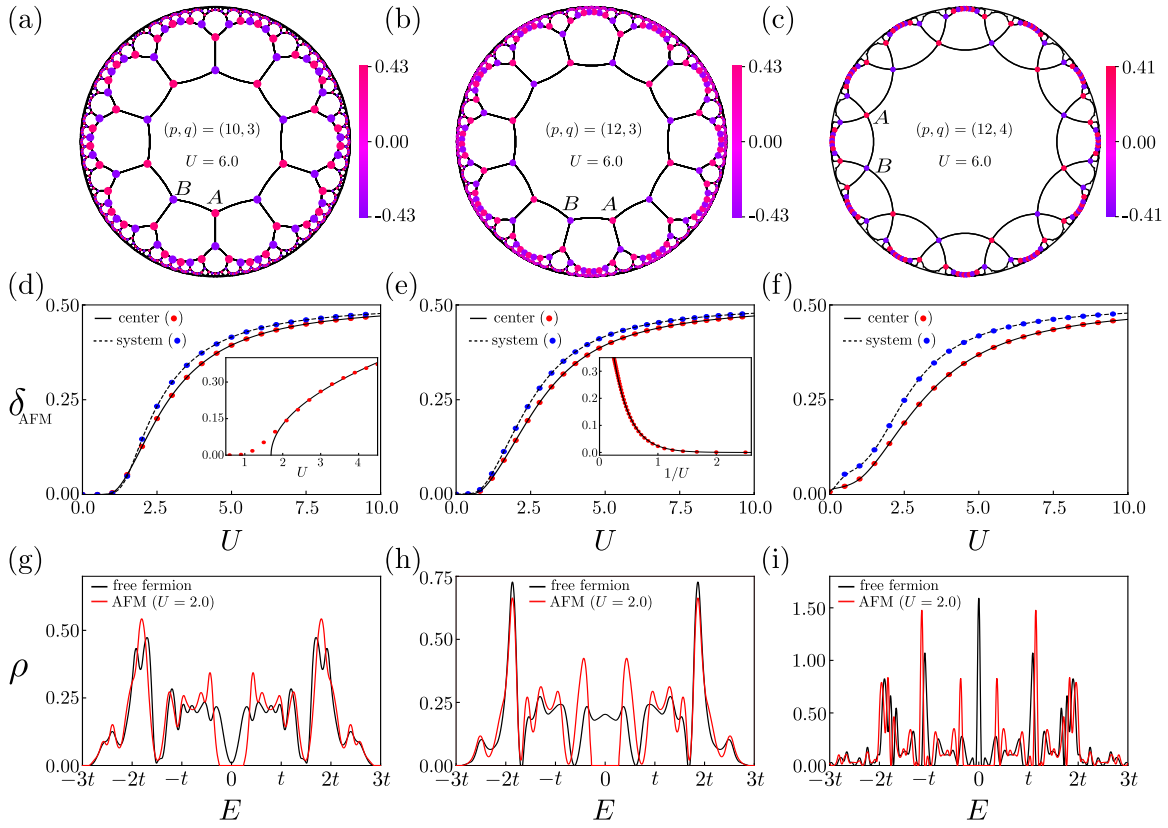


FIG. 2. On-site Hubbard repulsion (U) mediated AFM ordering [Eq. (9)] on HLs (shown on a Poincaré disk). Top row: Self-consistent solutions of magnetization at each site measured from its value at half-filling (zero), showing AFM order for $U = 6.0$. The results are presented for third generation $(10, 3)$, and second generation $(12, 3)$ and $(12, 4)$ HLs, respectively containing 2880, 972, and 1320 sites. All the other details are the same as in Fig. 1. The 'center' is constituted by the sites from the zeroth generation or center p-gon of the system [16].

lattice [16]. We numerically compute δ_A and δ_B, and subsequently $\delta_{\rm CDW}$ in the entire system with OBC for a wide range of V. See Fig. 1.

When δ_A and δ_B, thus $\delta_{\rm CDW}$ are finite in the entire system (not necessarily uniform), it becomes an insulator at half-filling by spontaneously breaking the sublattice symmetry. To appreciate this outcome, we define a two-component superspinor $\Psi^\top = (c_A, c_B)$, where c_A (c_B) is an N-dimensional spinor constituted by the annihilation operator on the sites from A (B) sublattice. In this basis, the tight-binding Hamiltonian and the CDW order-parameter are respectively

$$\hat{h}_0 = \begin{pmatrix} \mathbf{0} & \mathbf{t} \\ \mathbf{t}^\top & \mathbf{0} \end{pmatrix} \text{ and } \hat{h}_{\rm CDW} = \begin{pmatrix} \mathbf{\Delta} & \mathbf{0} \\ \mathbf{0} & -\mathbf{\Delta} \end{pmatrix} \equiv \hat{h}_\Delta, \quad (5)$$

where $\mathbf{0}$ is an N-dimensional null matrix, $\mathbf{t}$ is the inter-sublattice hopping matrix, and $\pm\mathbf{\Delta}$ are N-dimensional diagonal matrices, whose entries are the self-consistent solutions of δ_A and δ_B at various sites of the system, respectively, and $\top$ denotes transposition. As $\hat{h}_0$ and $\hat{h}_{\rm CDW}$ *anticommute* $\{\hat{h}_0, \hat{h}_{\rm CDW}\} = 0$, the CDW order acts like a mass for gapless fermions. Its spontaneous nucleation causes insulation near the charge neutrality point by opening a mass gap in the electronic spectra with vanishing [Fig. 1(g)], constant [Fig. 1(h)], and divergent [Fig. 1(i)] DOS at zero energy.

As $\rho(E) \sim |E|$ near the zero energy, condensation of the CDW on hyperbolic Dirac systems occurs beyond a critical NN repulsion (V_c), slightly away from which $\delta_{\rm CDW} \sim \sqrt{V - V_c}$ for $V > V_c$, allowing us to estimate V_c by minimizing the finite size effects [inset of Fig. 1(d)]. By contrast, when $\rho(0)$ is finite or divergent, the CDW order sets in for infinitesimal V. In the former system, CDW follows the BCS scaling $\delta_{\rm CDW} \sim \exp(-\kappa/V)$ due to a constant $\rho(0)$, further substantiated from the exponential fit between $\delta_{\rm CDW}$ and $1/V$ [inset of Fig. 1(e)]. On a $(12, 3)$ HL, the fitting parameter $\kappa = 2.36$. In the Supplemental Material (SM) we justify these scaling behaviors from the solutions of a gap equation [18, 21, 22]. When $\rho(0)$ is divergent, $\delta_{\rm CDW}$ grows considerably faster for weak V. Similar scaling holds on HLs with different $(p$ (even)$, q)$ [18]. With OBCs, $\delta_{\rm CDW}$ is not uniform, rather displays spatial modulations in the system [Fig. 1(a)-(c)]. However, a uniform CDW order with

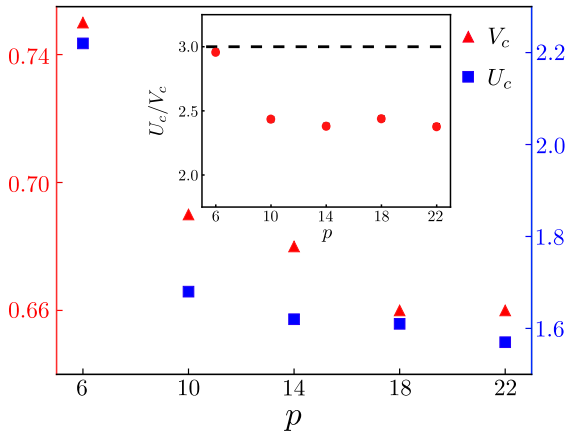


FIG. 3. Critical NN (V_c) and on-site (U_c) interactions for the CDW and AFM orderings, respectively, on graphene or Euclidean ($p = 6$) and hyperbolic ($p = 10, 14, 18, 22$) Dirac materials ($q = 3$), displaying their reduction with increasing p or curvature, indicating QPTs at weaker coupling on curved space. Inset: U_c/V_c in Dirac materials, expected to be locked at 3 (dashed line) in the mean-field limit.

$\delta_A = \delta_B = 0.5$ develops in the entire system when $V \gg 1$. In this limit, spinless fermions occupy one sublattice of bipartite HLs, while the other one is empty.

Hubbard model. Hubbard Hamiltonian with on-site repulsion (U) among spinful fermions (electrons) reads

$$H_U = U \sum_i \left(n_{i,\uparrow} - \frac{1}{2}\right)\left(n_{i,\downarrow} - \frac{1}{2}\right) - \mu N, \qquad (6)$$

where $n_{i,\uparrow/\downarrow}$ is the electronic density at site i with spin projection $\uparrow$ / $\downarrow$ in the z direction. The Hartree decomposition of H_U leads to

$$H_U^{\rm Har} = \sum_{x=A,B} \Big\{ \left(\langle n_{x,\uparrow}\rangle - \frac{1}{2}\right)\left(n_{x,\downarrow} - \frac{1}{2}\right) + \left(\langle n_{x,\downarrow}\rangle - \frac{1}{2}\right)\left(n_{x,\uparrow} - \frac{1}{2}\right)\Big\} - \mu N, \qquad (7)$$

where $\langle n_{A,\sigma}\rangle = 1/2 + \sigma\delta_{A,\sigma}(\boldsymbol{r})$, $\langle n_{B,\sigma}\rangle = 1/2 - \sigma\delta_{B,\sigma}(\boldsymbol{r})$, $\sigma = +/- \equiv \uparrow$ / $\downarrow$, and $\boldsymbol{r}$ measures the position of a site [21, 23]. Charge neutrality demands $\mu = 0$ and

$$\sum_{\sigma=\pm}\sum_{\boldsymbol{r}} \sigma\ [\delta_{A,\sigma}(\boldsymbol{r}) - \delta_{B,\sigma}(\boldsymbol{r})] = 0, \qquad (8)$$

which also keeps the average electronic density at each site equal to one. Then, an AFM ground state with $\delta_{A/B,\uparrow/\downarrow} > 0$ is characterized by the order-parameter

$$\delta_{\rm AFM} = \frac{1}{2}\left(\delta_{A,\uparrow} + \delta_{A,\downarrow} + \delta_{B,\uparrow} + \delta_{B,\downarrow}\right), \qquad (9)$$

where the B site is one of the two NN sites in the same generation of the hyperbolic lattice for a given site belonging to the A sublattice [16]. In noninteracting half-filled systems $\delta_{\rm AFM} = 0$. We follow the same numerical procedure to self-consistently compute $\delta_{\rm AFM}$ everywhere in the system, outlined in detail for the CDW order. The results are summarized in Fig. 2.

Inside the AFM phase, each site develops a finite magnetization, pointing in the opposite directions on two complementary sublattices. Consequently, the net magnetization in the system is zero. The AFM order also develops a mass gap near the half-filling, which can be appreciated in the following way. For spinful fermions, the tight-binding Hamiltonian $\hat{h}_0^{\rm spin} = \sigma_0 \otimes \hat{h}_0$ and AFM order $\hat{h}_{\rm AFM} = \sigma_3 \otimes \hat{h}_\Delta$ anticommute, $\{\hat{h}_0^{\rm spin}, \hat{h}_{\rm AFM}\} = 0$ [Eq. (5)]. Two-component Pauli matrices $\{\sigma_\mu\}$ operate on the spin indices. Hence, the AFM order also acts as a mass for gapless fermions and its nucleation causes insulation at half-filling. Scaling of the AFM order and its spatial variations are qualitatively similar to the ones for CDW. For instance, critical on-site repulsion for AFM order is $U_c = 1.68$ on $(10, 3)$ and the BCS fitting parameter $\kappa = 3.54$ on $(12, 3)$ HLs, respectively. And on $(12, 4)$ HL the AFM develops rapidly for weak U.

Weak coupling QPT. The critical couplings for CDW and AFM orders on hyperbolic Dirac materials ($q = 3$) decrease monotonically with increasing p or the curvature, compared to the honeycomb lattice, harboring Dirac fermions on Euclidean flat land [Fig. 3], where $V_c \approx 0.75$ [19, 24] and $U_c \approx 2.22$ [25], which we also reproduce. It strongly indicates curvature induced QPTs at weaker coupling for Dirac fermions on curved space. Within the mean-field approximation U_c/V_c is expected to be 3, as the NN repulsion is operative between the fermionic densities on three pairs of NN sites, while the Hubbard repulsion is on-site. On hyperbolic lattices with OBC although $U_c/V_c \approx 2.4$ remains approximately constant, it is smaller than 3 [Fig. 3 (inset)], possibly due to a rapidly increasing large number of sites at the boundary of the system with only two NN sites, increasing V_c.

Summary and discussion. From numerical Hartree self-consistent analyses, we show that NN Coulomb and on-site Hubbard repulsions respectively support CDW and AFM orders on half-filled bipartite HLs. While in Dirac systems such orderings take place through a QPT at finite interactions, they nucleate even for infinitesimal V and U when the DOS at half-filling is either finite or divergent. The Fock term for the NN interaction $\langle c_i^\dagger c_j\rangle$ renormalizes the NN hopping amplitude, leaving the system gapless. As such any other decomposition of these interactions yields only gapless states, which are energetically inferior to the fully and isotropic gapped CDW and AFM states at zero temperature (no competition with entropy). From (a) the generation dependence of the local CDW and AFM orders on HLs with different system sizes, and (b) local DOS at its various generations, we show that the dynamic symmetry breaking takes place everywhere in the system and the entire system then becomes correlated insulator [18]. From numerical solutions of the Dyson equation [26], we show that

mean-field solutions for the CDW is stable against Gaussian fluctuations around it [18], which can be generalized for the amplitude mode of the AFM order, leaving aside its two gapless Goldstone modes. Due to a genuine 2D nature of the HLs, in which the ratio of edge to bulk sites reaches a finite number [27], the Goldstone modes in the AFM order do not destroy any long-range order at zero temperature. Due to the two-dimensional nature of the hyperbolic lattices, the gravitational anomaly is absent therein and it does not impede our outcomes [28]. Also, on hyperbolic Dirac materials the critical interactions for these two orders decrease with increasing curvature or p. These predictions can be further tested from quantum Monte Carlo simulations, accounting for quantum fluctuations, as shown for Euclidean Dirac systems (graphene) with on-site [29, 30] and NN [31, 32] repulsions. The universality class of the QPTs to CDW and AFM phases cab be captured by Gross-Neveu [33] or Nambu-Jona-Lasinio [34] models for dynamic mass generation on curved space [35], endowing an unique opportunity to test the predictions of curved space quantum field theory directly from HL based numerical investigations. In future, we will search for other exotic correlated quantum phases on HLs, among which topological Mott insulators and superconductors are the fascinating ones.

Designer electronic materials [36–40] and cold atomic setups are promising platforms where our predicted quantum phases can be observed experimentally. A curved designer material can be engineered by growing its substrate (typically Cu) on another material with a different thermal expansion coefficient. When such a heterostructure is cooled down, the Cu substrate gets curved, which then can be decorated by the sites of desired HLs. With tunable hopping amplitudes t, the ratios V/t and U/t can be adjusted on hyperbolic designer quantum materials to trigger various quantum orders. In cold atomic setups, desired hyperbolic tessellations can be achieved by suitable arrangements of laser traps. In such systems, at least on-site Hubbard repulsion can be tuned to realize AFM order, as recently demonstrated on various Euclidean lattices [41–44].

Acknowledgments. N.G. and B.R. were supported by a Startup grant of B.R. from Lehigh University. S.M. was supported by Weizmann Institute of Science, Israel Deans fellowship through Feinberg Graduate School and Raymond and Beverly Sackler Center for Computational Molecular and Material Science at Tel Aviv University. We are thankful to the Divisional Associate Editor of this paper, Alexander Altland, for constructive criticism.

* Equal contributors
† Corresponding author: bitan.roy@lehigh.edu

[1] F. Sausset and G. Tarjus, Periodic boundary conditions on the pseudosphere, Journal of Physics A Mathematical General **40**, 12873 (2007).
[2] A. J. Kollár, M. Fitzpatrick, and A. A. Houck, Hyperbolic lattices in circuit quantum electrodynamics, Nature (London) **571**, 45 (2019).
[3] M. Asaduzzaman, S. Catterall, J. Hubisz, R. Nelson, and J. Unmuth-Yockey, Holography on tessellations of hyperbolic space, Phys. Rev. D **102**, 034511 (2020).
[4] I. Boettcher, P. Bienias, R. Belyansky, A. J. Kollár, and A. V. Gorshkov, Quantum simulation of hyperbolic space with circuit quantum electrodynamics: From graphs to geometry, Phys. Rev. A **102**, 032208 (2020).
[5] R. C. Brower, C. V. Cogburn, A. L. Fitzpatrick, D. Howarth, and C.-I. Tan, Lattice setup for quantum field theory in AdS_2, Phys. Rev. D **103**, 094507 (2021).
[6] J. Maciejko and S. Rayan, Hyperbolic band theory, Sci. Adv. **7**, eabe9170 (2021).
[7] K. Ikeda, S. Aoki, and Y. Matsuki, Hyperbolic band theory under magnetic field and Dirac cones on a higher genus surface, J. Phys.: Condens. Matter **33**, 485602 (2021).
[8] I. Boettcher, A. V. Gorshkov, A. J. Kollár, J. Maciejko, S. Rayan, and R. Thomale, Crystallography of hyperbolic lattices, Phys. Rev. B **105**, 125118 (2022).
[9] N. Cheng, F. Serafin, J. McInerney, Z. Rocklin, K. Sun, and X. Mao, Band Theory and Boundary Modes of High-Dimensional Representations of Infinite Hyperbolic Lattices, Phys. Rev. Lett. **129**, 088002 (2022).
[10] J. Maciejko and S. Rayan, Automorphic Bloch theorems for hyperbolic lattices, Proc. Natl. Acad. Sci. **119**, e2116869119 (2022).
[11] A. Attar and I. Boettcher, Selberg trace formula in hyperbolic band theory, Phys. Rev. E **106**, 034114 (2022).
[12] R. Mosseri, R. Vogeler, and J. Vidal, Aharonov-Bohm cages, flat bands, and gap labeling in hyperbolic tilings, Phys. Rev. B **106**, 155120 (2022).
[13] T. Bzdušek and J. Maciejko, Flat bands and band-touching from real-space topology in hyperbolic lattices, Phys. Rev. B **106**, 155146 (2022).
[14] E. Kienzle and S. Rayan, Hyperbolic band theory through Higgs bundles, Adv. Math. **409**, 108664 (2022).
[15] A. Stegmaier, L. K. Upreti, R. Thomale, and I. Boettcher, Universality of Hofstadter Butterflies on Hyperbolic Lattices, Phys. Rev. Lett. **128**, 166402 (2022).
[16] Sites belonging to the center p-gon constitute the zeroth generation and each successive layers of sites constitute the progressively next generations of hyperbolic lattices. The sites from the zeroth generation or center p-gon of the system is also coined 'center' in Figs. 1 and 2.
[17] A. P. Schnyder, S. Ryu, A. Furusaki, and A. W. W. Ludwig, Classification of topological insulators and superconductors in three spatial dimensions, Phys. Rev. B **78**, 195125 (2008).
[18] See Supplemental Materials at XXX-XXXX for (a) symmetry classification of free spinless fermion tight-binding model, (b) solution of a gap equation, (c) self-consistent CDW and AFM orders in other bipartite hyperbolic lattices, (d) computation of the DOS in hyperbolic Dirac liquids from hyperbolic band theory, (e) finite size effects of the CDW and AFM order, and (f) Gaussian fluctuation of the CDW order around mean-field solutions.
[19] B. Roy and I. F. Herbut, Inhomogeneous magnetic catalysis on graphene's honeycomb lattice, Phys. Rev. B **83**,

195422 (2011).
[20] B. Roy and J. D. Sau, Competing charge-density wave, magnetic, and topological ground states at and near Dirac points in graphene in axial magnetic fields, Phys. Rev. B **90**, 075427 (2014).
[21] B. Roy, Interacting nodal-line semimetal: Proximity effect and spontaneous symmetry breaking, Phys. Rev. B **96**, 041113 (2017).
[22] M. Tinkham, *Introduction to Superconductivity* (Dover Publication, New York, 2004).
[23] B. Roy, F. F. Assaad, and I. F. Herbut, Zero Modes and Global Antiferromagnetism in Strained Graphene, Phys. Rev. X **4**, 021042 (2014).
[24] C. Weeks and M. Franz, Interaction-driven instabilities of a Dirac semimetal, Phys. Rev. B **81**, 085105 (2010).
[25] S. Sorella and E. Tosatti, Semi-Metal-Insulator Transition of the Hubbard Model in the Honeycomb Lattice, Europhysics Letters (EPL) **19**, 699 (1992).
[26] A. L. Fetter and J. D. Walecka, *Quantum Theory of Many-Particle Systems* (Dover Publication, Mineola, New York, 2003).
[27] S. Yu, X. Piao, and N. Park, Topological Hyperbolic Lattices, Phys. Rev. Lett. **125**, 053901 (2020).
[28] K. Fujikawa and H. Suzuki, *Path Integrals and Quantum Anomalies* (Oxford University Press, Oxford, 2004).
[29] F. F. Assaad and I. F. Herbut, Pinning the Order: The Nature of Quantum Criticality in the Hubbard Model on Honeycomb Lattice, Phys. Rev. X **3**, 031010 (2013).
[30] Y. Otsuka, S. Yunoki, and S. Sorella, Universal Quantum Criticality in the Metal-Insulator Transition of Two-Dimensional Interacting Dirac Electrons, Phys. Rev. X **6**, 011029 (2016).
[31] L. Wang, P. Corboz, and M. Troyer, Fermionic quantum critical point of spinless fermions on a honeycomb lattice, New J. Phys. **16**, 103008 (2014).
[32] Z.-X. Li, Y.-F. Jiang, and H. Yao, Fermion-sign-free Majarana-quantum-Monte-Carlo studies of quantum critical phenomena of Dirac fermions in two dimensions, New J. Phys. **17**, 085003 (2015).
[33] D. J. Gross and A. Neveu, Dynamical symmetry breaking in asymptotically free field theories, Phys. Rev. D **10**, 3235 (1974).
[34] Y. Nambu and G. Jona-Lasinio, Dynamical Model of Elementary Particles Based on an Analogy with Superconductivity. I, Phys. Rev. **122**, 345 (1961).
[35] I. L. Buchbinder, S. D. Odintsov, and I. L. Shapiro, Renormalization group approach to quantum field theory in curved space-time, Riv. Nuovo Cim. **12**, 1 (1989).
[36] K. K. Gomes, W. Mar, W. Ko, F. Guinea, and H. C. Manoharan, Designer Dirac fermions and topological phases in molecular graphene, Nature (London) **483**, 306 (2012).
[37] M. Polini, F. Guinea, M. Lewenstein, H. C. Manoharan, and V. Pellegrini, Artificial honeycomb lattices for electrons, atoms and photons, Nature Nanotech **8**, 625 (2013).
[38] L. C. Collins, T. G. Witte, R. Silverman, D. B. Green, and K. K. Gomes, Imaging quasiperiodic electronic states in a synthetic Penrose tiling, Nat. Commun. **8**, 15961 (2017).
[39] S. N. Kempkes, M. R. Slot, S. E. Freeney, S. J. M. Zevenhuizen, D. Vanmaekelbergh, I. Swart, and C. M. Smith, Design and characterization of electrons in a fractal geometry, Nat. Phys. **15**, 127 (2019).
[40] S. N. Kempkes, M. R. Slot, J. J. van den Broeke, P. Capiod, W. A. Benalcazar, D. Vanmaekelbergh, D. Bercioux, I. Swart, and C. Morais Smith, Robust zero-energy modes in an electronic higher-order topological insulator, Nat. Mater. **18**, 1292 (2019).
[41] T. Esslinger, Fermi-Hubbard Physics with Atoms in an Optical Lattice, Annu. Rev. Condens. Matter Phys. **1**, 129 (2010).
[42] T. Uehlinger, G. Jotzu, M. Messer, D. Greif, W. Hofstetter, U. Bissbort, and T. Esslinger, Artificial Graphene with Tunable Interactions, Phys. Rev. Lett. **111**, 185307 (2013).
[43] L. W. Cheuk, M. A. Nichols, K. R. Lawrence, M. Okan, H. Zhang, E. Khatami, N. Trivedi, T. Paiva, M. Rigol, and M. W. Zwierlein, Observation of spatial charge and spin correlations in the 2D Fermi-Hubbard model, Science **353**, 1260 (2016).
[44] A. Mazurenko, C. S. Chiu, G. Ji, P. M. F., M. Kanász-Nagy, R. Schmidt, F. Grusdt, E. Demler, D. Greif, and M. Greiner, A cold-atom Fermi–Hubbard antiferromagnet, Nature (London) **545**, 462 (2017).